ANALYSIS OF PELLET-CLAD INTERACTION OF LWR FUEL RODS DURING POWER RAMPS

A. R. Massih
Quantum Technologies AB
SE-75183 Uppsala, Sweden
Phone: +46-70-3089590
Fax: +46-18-509890
E-mail: alma@quantumtech.se

L. O. Jernkvist
Quantum Technologies AB
SE-75183 Uppsala, Sweden
Phone: +46-18-509690
E-mail: loje@quantumtech.se

J. E. Lindbäck*
Westinghouse Electric Sweden AB
SE-72163 Västerås, Sweden
Phone: +46-8-6988498
E-mail: janerik.lindback@ski.se

G. Zhou
Westinghouse Electric Sweden AB
SE-72163 Västerås, Sweden
Phone: +46-21-347236
E-mail: gang.zhou@se.westinghouse.com

ABSTRACT

A computational method is employed to analyse the pellet-clad interaction phenomenon of light water reactor fuel under power ramps. The pellet-clad contact model used accounts for friction and soft/hard contact due to fragmented (relocated) fuel pellets. Zircaloy cladding is assumed as elastic-plastic-viscoplastic material with irradiation hardening, obeying the Levy-Mises associated plasticity law. The effect of iodine-induced stress corrosion cracking is described by using a fracture mechanics-based model for crack propagation. These models are employed to evaluate some power ramp experiments made on boiling water reactor (BWR) and pressurised water reactor (PWR) fuel rods. In particular, we analyse ramp tests made on a 10×10 BWR rod equipped with Zr-Sn liner pre-irradiated in a commercial BWR to a rod exposure of around 32 MWd/kgU; and two 17×17 PWR rods, pre-irradiated in a commercial PWR to a rod exposure of around 27 MWd/kgU. The peak linear power densities reached under ramping (ramp terminal level, RTL) for the two PWR rods were 48 and 41 kW/m, respectively. The former rod failed after 5 minutes at RTL of 48 kW/m, whereas the latter rod survived the ramp and a hold time of 12 h at 41 kW/m. The BWR rod survived the test at RTL of 57 kW/m and a hold time of 12 h. The tests demonstrate the capability of lined cladding to withstand high RTL. For these tests, clad deformations and stresses during ramps are calculated and the results are compared with measured data. The causes of failure and survival are discussed and analysed with the aid of computations. Also, fuel pellet swelling and fission product gas release for the rods are calculated and the results are compared with measured data.

Keywords: PCI analysis; Light water reactor fuel; Power ramp test.

1 INTRODUCTION

Pellet-clad interaction (PCI) is a major concern in fuel rod design and reactor core operation in light water reactors (LWRs), since it may cause fuel cladding fracture during reactor operation. PCI-induced failure is associated with iodine stress corrosion cracking (SCC) of zirconium alloy clad and has been observed upon variations in linear power density (i.e. power per unit length of rod). It is caused by a combination of stresses in the clad due to the pellet-clad contact pressure and chemical reaction of corrosive fission products, such as iodine released during service, with Zr alloy under a power ramp. In fact an early observation in the Main Yankee pressurised water reactor (PWR) indicated that damaging interaction between the fuel pellet UO_2 and Zircaloy cladding did not have

*Current address: Swedish Nuclear Power Inspectorate, SE-10658 Stockholm, Sweden.

to follow large or rapid power changes; it could also occur in the low stress highly corrosive (from fission product) condition caused by pellet-clad gap heat transfer degradation (Fuhrman, Pasupathi and Scott 1976) & (Fuhrman, Pasupathi and Corsetti 1977).

PCI has been a topic of numerous experimental and computational studies with a great amount of accumulated field experience. This has lead to PCI-resistant designs and operation guidelines, which have significantly reduced the propensity for such failures in recent years. In particular, the introduction of Zr-lined clad has effectively mitigated PCI in boiling water reactors (BWRs) and has provided a high degree of operational flexibility (Armijo, Coffin and Rosenbaum 1994). Liner consists of a thin layer of "pure" zirconium or dilute Zr alloy metallurgically bonded to the inner surface of Zircaloy-2 cladding tube. The liner thickness is about 10% of the clad wall thickness. The PCI resistance of liner material is attributed to its higher ductility than Zircaloy, and more importantly, its much higher resistance to iodine-induced SCC.

Westinghouse Electric Sweden (former ABB Atom) has performed extensive power ramp testing on pre-irradiated BWR and PWR fuel pins in the Studsvik R2 reactor in the past decades, in order to understand the PCI phenomenon and to improve the PCI resistance of fuel rods, including development of advanced liner for BWR cladding tubes (Massih, Hallstadius and Vesterlund 1987). Overviews, from industrial perspective, on PCI testing and computations relating to LWR fuels can be found in (Gärtner and Fischer 1987) & (Massih, Rajala and Jernkvist 1995). Cox (1990) has reviewed the PCI failure mechanism in detail. A brief overview of the subject from materials' standpoint is given by Edsinger and Murthy (2001). More recent modelling and analyses on both structural and fracture aspects of PCI are given in (Zhou, Lindbäck, Schutte, Jernkvist and Massih 2004) and (Billaux 2004).

In this paper, we evaluate some power ramp experiments made on BWR and PWR fuel rods in the Studsvik R2 test reactor. In particular, we analyse a recent test made on a Westinghouse 10×10 BWR rod with a lined clad, pre-irradiated in a commercial BWR, and earlier tests made on two ABB Atom 17×17 PWR rods, pre-irradiated in a commercial PWR. The pellet-clad contact model used in our evaluation accounts for friction and soft/hard contact due to fragmented (relocated) fuel pellets. The effect of the iodine-induced stress corrosion cracking is described by using a fracture mechanics-based model for crack propagation following Jernkvist (1995).

The plan of this paper is as follows: First, we outline the principal PCI models used in our analysis. Next, the ramp tests under consideration are briefly described, followed by the results of our computations on these tests. Finally, we evaluate the results of our computations in light of the experimental data and the models used.

2 MODELS

The PCI computational method used in our work consists of three principal constituents; namely, mechanics of PCI, kinetics of iodine release from fuel and a model for clad failure. Mechanics of PCI describes the contact forces and the pellet-clad deformations that arise under interfacial interactions. Iodine release is intimately connected to fission product gas release from fuel to the rod internal volume. It constitutes the chemical parts of the PCI effect. The combined results of the pellet-clad mechanical interaction and chemical reaction (released iodine and zirconium alloy) are used to model stress corrosion crack propagation in the clad and to predict its eventual failure. In the following subsections these models are briefly described.

2.1 Mechanics of PCI

The pellet cladding mechanical interaction (PCMI) model used here includes the effect of friction and axial mechanical interaction and associated rod elongation. The UO_2 fuel pellet is considered as rigid, but can deform by thermal expansion, densification, fission product swelling and cracking (relocation). The pellet radial (normal) displacement is expressed as: $u_n^p = u_T + u_D + u_S + u_R$, where u_T, u_D, u_S, and u_R are the radial pellet displacement due to thermal expansion, fuel densification, swelling, and relocation, respectively. UO_2 fuel pellets crack during power variation, caused by sharp temperature gradient. Pellet fragments can relocate, due to flow-induced vibration of fuel rod, and hence reduce the pellet-clad gap size. Pellet radial displacement u_R due to relocation is assumed to be a function of the radial contact pressure P_n defined as

$$u_R = H(P_n^m - P_n)\mathrm{R}^m\left(1 - \frac{P_n}{P_n^m}\right), \tag{1}$$

where R^m is the maximum pellet relocation, i.e. under zero contact pressure condition, and P_n^m is the minimum contact pressure to fully remove the relocation, $u_R = 0$ (Forsberg and Massih 1989). Here $H(x)$ the Heaviside function; $H(x) = 0$ if $x < 0$ and $H(x) = 1$ if $x > 0$. Pellet relocation in the axial direction is not considered.

A finite element (FE) method is used to calculate stresses and strains in the clad in the radial, axial (r,z) coordinates. The FE model assumes that the clad tube is an axisymmetric shell. The clad material is a zirconium alloy and it deforms by thermal expansion, elastic-plastic deformation and creep (viscoplastic deformation). The following assumptions are made in the mechanical model for the clad: (i) The clad tube is divided axially, along the z-coordinate, into a number of segments. (ii) Within each segment, stresses and strains are spatially constant. (iii) Within each segment, the axial displacement $v(r_j,z_j)$ is independent of radius r. (iv) Within each segment, the radial displacement $u(r_j,z_j)$ is independent of z.

The constitutive relation for zirconium alloy clad that include thermo-elasticity, plasticity, and creep is written as: $\sigma = \mathbf{D}(\varepsilon_m - d\varepsilon_p)$, where $\varepsilon_m = \varepsilon - \varepsilon_p + d\varepsilon_p - \varepsilon_c - \varepsilon_T = \varepsilon_e + d\varepsilon_p$ is the modified elastic strain tensor and σ is the stress tensor. Here, ε is the total strain tensor, ε_p the total accumulated plastic strain, $d\varepsilon_p$ the increment of plastic strain, ε_c include other strains (creep, irradiation growth), ε_T the thermoelastic strain, ε_e the elastic strain and D is the elasticity matrix. The yield stress of Zr alloy cladding is a function of strain, temperature and neutron fluence. If yielding occurs, the plastic strain increment $d\varepsilon_p$ is calculated through the Levy-Mises flow rule of associated plasticity. Isotropic hardening is assumed. For material properties of UO_2 and Zircaloy, we have employed the correlations given in (Hagrman and Reyman 1979), for Zircaloy creep (Limbäck and Andersson 1996) and pellet relocation (Forsberg and Massih 1989).

The pellet-clad gap, defined as: $\mathbf{G} = \mathbf{G}^0 + \mathbf{u}^c - \mathbf{u}^p$, where for each pellet-clad node-pair in the FE-model, $\mathbf{G} = (G_n, G_t)$ is the current gap size, $\mathbf{G^0} = (G_n^0, 0)$ the initial gap, $\mathbf{u}^p = (u_n^p, u_t^p)$ the pellet outer surface displacement, $\mathbf{u}^c = (u_n^c, u_t^c)$ the clad inner surface displacement; and the subscripts n and t denote the radial (normal) and the axial (tangential) gap components, respectively.

The state of the gap is governed by the open-stick (*Kuhn-Tucker*) condition

$$\begin{cases} P_n \geq 0, & \text{compressibility} \\ G_n \geq 0, & \text{impenetrability} \\ P_n G_n = 0. & \text{complementarity} \end{cases} \tag{2}$$

Upon pellet-clad contact, the radial mechanical gap becomes zero and friction forces between the pellet and clad are generated. These friction forces (or stresses) are assumed to follow the Amontons-Coulomb friction laws, which state: (i) the friction force is proportional to normal load, (ii) the friction force is independent of the apparent area of contact, (iii) the friction force is independent of the sliding velocity, implying that the force required to initiate sliding will be the same as the force needed to maintain sliding at any specific velocity. Let P_t be the axial (tangential) friction contact stress and μ the friction coefficient, the stick-slip conditions for $G_n = 0$ and $P_n < 0$ are:

$$|P_t| \leq \mu P_n; \qquad P_t = \text{sgn}(\Delta G_t)\mu P_n, \tag{3}$$

where the first relation from the left designates the stick condition, while the second one the slip condition. Here, ΔG_t indicates the change in axial (tangential) gap component G_t. The algorithm for calculating the states of gap and contact was developed by H. Schutte and is outlined in (Zhou et al. 2004).

2.2 Iodine release

Stable and long-lived isotopes of iodine (^{127}I, ^{129}I) are assumed to be released from the fuel pellets by the same processes as for the noble gases Xe and Kr. The release of these gaseous fission products is modelled by assuming that UO_2 consists of spherical grains of equal size (Speight 1969). The fission product gases are produced at a rate $\beta(t)$ in a grain of radius $R(t)$. The gases migrate to grain boundaries by diffusion with a diffusion coefficient $D(t)$. The gas atoms reaching the boundaries precipitate into intergranular bubbles with a local area density of $N(t)$ (per unit area) and a grain boundary re-solution rate of $B(t) = b\lambda/2$, where b is the grain boundary re-solution frequency, and $\lambda/2$ the re-solution depth from the grain face. All these variables are assumed to be time-dependent. The concentration of gas atoms at position r at time t in the grain, $C(r,t)$, is described by the diffusion equation:

$$\frac{\partial C(r,t)}{\partial t} = D(t)\nabla^2 C(r,t) + \beta(t), \quad \text{for} \quad 0 < r < R(t). \tag{4}$$

The imposed boundary conditions to Eq. (4) are $\partial C(0,t)/\partial r = 0$ and $C(R,t) = B(t)N(t)/D(t)$, with the initial condition $C(r,0) = 0$. When the gas concentration at the grain boundary, $N(t)$, reaches a certain saturation level,

N_s, gas is assumed to be released to the rod free volume. The gas atom density at saturation N_s is calculated through the equation of state for ideal gases. Gas diffusion and grain growth may occur simultaneously, and analytical solutions to the problem of gas diffusion in an expanding medium are therefore used to solve Eq. (4) (Forsberg and Massih 2001).

2.3 Stress corrosion cracking of non-liner fuel

For fuel rods with conventional non-liner Zircaloy cladding, the combined effects of mechanical and chemical interaction with the fuel pellets may cause failure of the clad tube through iodine-induced stress corrosion cracking. This kind of failure is predicted with a model, in which the propagation of stress corrosion cracks is treated by use of linear elastic fracture mechanics (LEFM). The cracks are supposed to nucleate at pre-existing flaws at the clad inner surface, which are subjected to local stress concentrations induced by the opening of radial pellet cracks; see Fig. 1. The initial clad flaws, which are typically $\approx 10\,\mu$m deep (Ohara, Nomata, Irube, Iwata and Futakuchi 1994), are assumed to start growing transgranularly, provided that the stress intensity at the tip of the flaw exceeds a critical threshold and that the clad material is chemically sensitised and thus susceptible to SCC; the latter condition is cast in the form of a threshold iodine concentration in the pellet-clad gap. The transgranular crack growth rate is in our model correlated to temperature, crack tip stress intensity K_I, and iodine concentration C_I at the clad inner surface through

$$\frac{da}{dt} = F(C_I)\ln\left(\frac{K_I}{K_{ISCC}(T)}\right), \quad \text{for} \quad K_I > K_{ISSC}. \tag{5}$$

Here, a is the crack length, F is a function of the iodine concentration C_I, and K_{ISCC} is the temperature-dependent threshold stress intensity for transgranular SCC. The correlations for F and K_{ISCC} are based on more than 100 out-of-pile fracture mechanics tests, made on both irradiated and unirradiated clad tubes under controlled temperature and iodine environment. The database comprises recrystallised Zircaloy-2 as well as stress relieved annealed Zircaloy-4 clad materials (Jernkvist 2005).

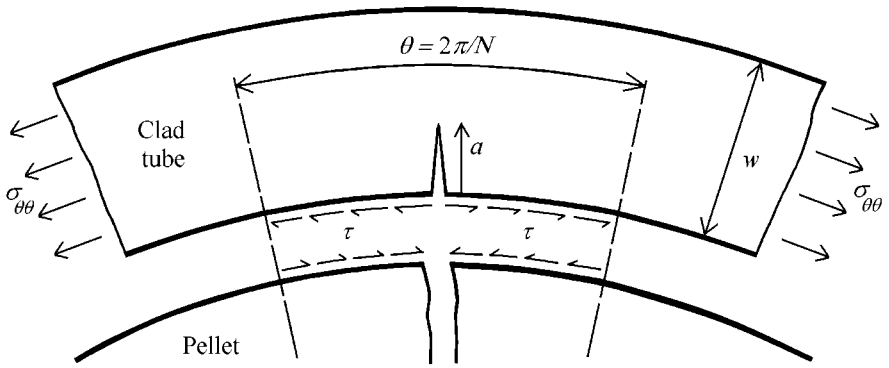

Figure 1. A schematic drawing showing a portion of N symmetrically spaced radial cracks in a fuel pellet; the geometry considered in our model. When the cracked fuel pellet expands, the clad experiences local shear stresses from pellet-clad sliding, $\tau = \mu P_n$, where μ is the coefficient of pellet-clad friction and P_n is the pellet-clad normal pressure.

The incremental crack growth in each time step of an analysis is evaluated through Eq. (5) for each axial segment of the fuel rod. The stress intensity factor is estimated from the current crack length, pellet-clad contact pressure and clad average hoop stress through superposition of analytical solutions

$$K_I = \frac{\tau R_i \theta}{\sqrt{\pi a}} f_1\left(\frac{R_i\theta}{2a}\right) f_2\left(\frac{a}{w}\right) + \sigma_{\theta\theta}\sqrt{\pi a}\, f_3\left(\frac{a}{w}, \frac{R_i}{w}\right). \tag{6}$$

Here, f_1, f_2 and f_3 are dimension-free functions and R_i is the clad inner radius; other parameters are defined in Fig. 1. The first term on the right-hand-side of Eq. (6) accounts for the local effect of frictional shear forces ($\tau \equiv P_t = \mu P_n$) from the pellet, whereas the second term is related to the uniform loading in the hoop direction ($\sigma_{\theta\theta}$).

2.4 Ductile failure of liner fuel

Liner has proven to be an effective remedy for avoiding fuel rod failures caused by iodine-induced SCC. In comparison with the Zircaloy base material of the clad tube, the liner material has a lower content of alloying elements and a much lower susceptibility to iodine-induced SCC. The liner currently used by Westinghouse in BWR fuel rods contains tin and small amounts of iron as alloying elements (Zr-0.3Sn-0.05Fe-0.05O by wt%), see (Dahlbäck, Halstadius and Limbäck 2004). The resistance to iodine-induced SCC of this material has been confirmed both by ramp tests and by out-of-pile mechanical property tests (Massih et al. 1987), and the results clearly show that the Westinghouse Zr-Sn liner is practically immune to iodine-induced SCC. We therefore assume that the survivability of fuel rods equipped with this kind of liner under PCI is limited by irradiation- and hydrogen-induced embrittlement of the clad tube, and not by SCC. Consequently, a strain-based failure criterion is applied. Clad tube failure is assumed to take place when the calculated clad hoop plastic strain $\varepsilon^{p}_{\theta\theta}$ exceeds a threshold value ε_f, which is correlated to clad temperature T, strain rate $\dot{\varepsilon}_{\theta\theta}$, hydrogen content c_H, and fast neutron fluence ϕ, on a best-estimate basis. Hence, we postulate that a clad tube with liner fails when

$$\varepsilon^{p}_{\theta\theta} \geq \varepsilon_f(T, \dot{\varepsilon}_{\theta\theta}, c_H, \phi), \quad \text{and} \quad \dot{\varepsilon}^{p}_{\theta\theta} > 0. \tag{7}$$

The correlation for the failure strain ε_f is derived from more than 200 out-of-pile mechanical property tests, made on irradiated clad tubes, as well as on un-irradiated hydrogen-charged tube samples. A full description of this failure criterion and its experimental support can be found in (Jernkvist, Massih and Rudling 2004).

3 RAMP TESTS

We have used the models described in the foregoing section to evaluate some power ramp experiments in the Studsvik R2 test reactor, made on pre-irradiated PWR and BWR fuel rods. In particular, we analyse ramp tests made on two 17×17 PWR rods, pre-irradiated in a commercial PWR, and a test made on a 10×10 BWR rod with a lined clad pre-irradiated in a commercial BWR. The BWR test results were partly presented in an earlier seminar (Zhou et al. 2004), where a preliminary computer simulation was reported.

3.1 BWR test

The considered test was conducted on a Westinghouse 10×10 SVEA-96S fuel assembly rod, base irradiated in the Barsebäck 2 BWR in Sweden, during 1999-2002, to a rod exposure of about 32 MWd/kgU (this is the number of megawatt days of thermal energy released by fuel containing 1 kg of uranium atoms). The irradiation history of the rod, the linear power density vs. irradiation time, is depicted in Fig. 2.

A test pin (designated here as W-pin 33002) of length 570 mm with UO_2 fuel pellets was disassembled from the original (segmented) rod for power ramp testing in the Studsvik R2 reactor. Basic technical data on the fuel pin are given in Table 1. The pin was non-destructively examined in hot cell at Studsvik. Examination covered pin diameter measurements and γ-spectrometry. The R2 test facility and experimental technique for fuel ramp test is described in (Carlsson and Engman 1999). For the considered test, a pressurised water loop was used for simulating BWR coolant conditions (9 MPa, 558 K). The rod surface temperature was limited by sub-cooled surface boiling, implying that the rod surface temperature may not exceed the saturation temperature (576 K) by more than a few degrees.

The pin was subjected to irradiation in R2 by first raising the linear power density or linear heat generation rate (LHGR, i.e. power per unit length of rod) from zero to 12 kW/m very rapidly. This initial power step was followed by a slow power increase during a period of 25 minutes until the conditioning LHGR of 22.5 kW/m was reached. Conditioning means that a fuel pin reaches a state of thermo-mechanical equilibrium at a constant LHGR after a sufficient period of time; in this case about 12 h. After conditioning, the pin was subjected to a power ramp, where a ramp step height of around 5 kW/m and a step duration of 1 h were utilised. The step ramp rate was about 6.4 kW/m/min. Moreover, the ramp terminal level (RTL) was around 56.5 kW/m. Power was held at RTL for about 12 h, then LHGR was finally reduced to 7 kW/m after 50 minutes, upon which the irradiation was terminated. The pin survived the ramp. Fig. 3 shows the power history during the ramp test.

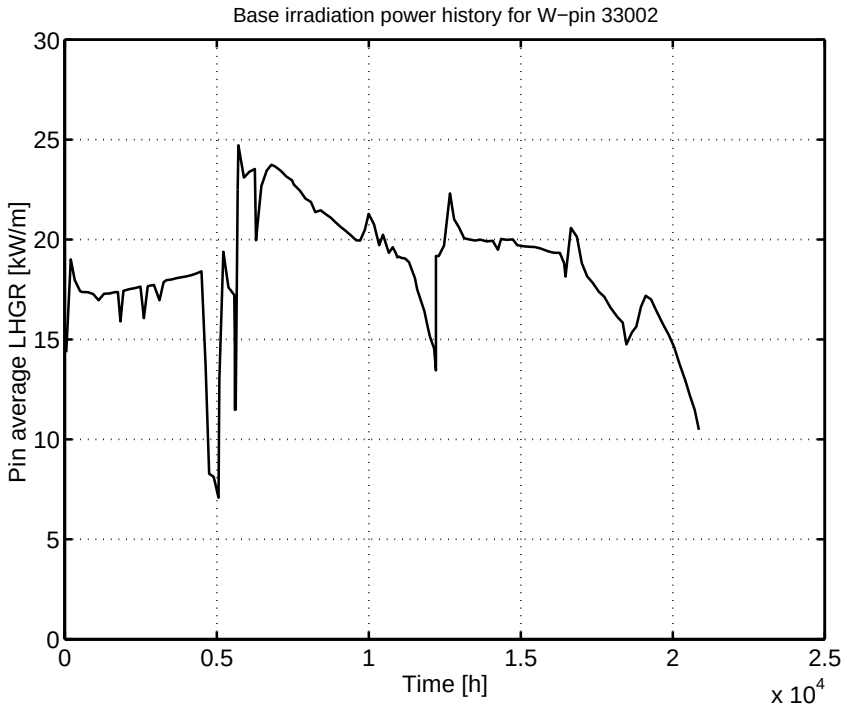

Figure 2. Base power history for the BWR rod irradiated in the Barsebäck 2 reactor.

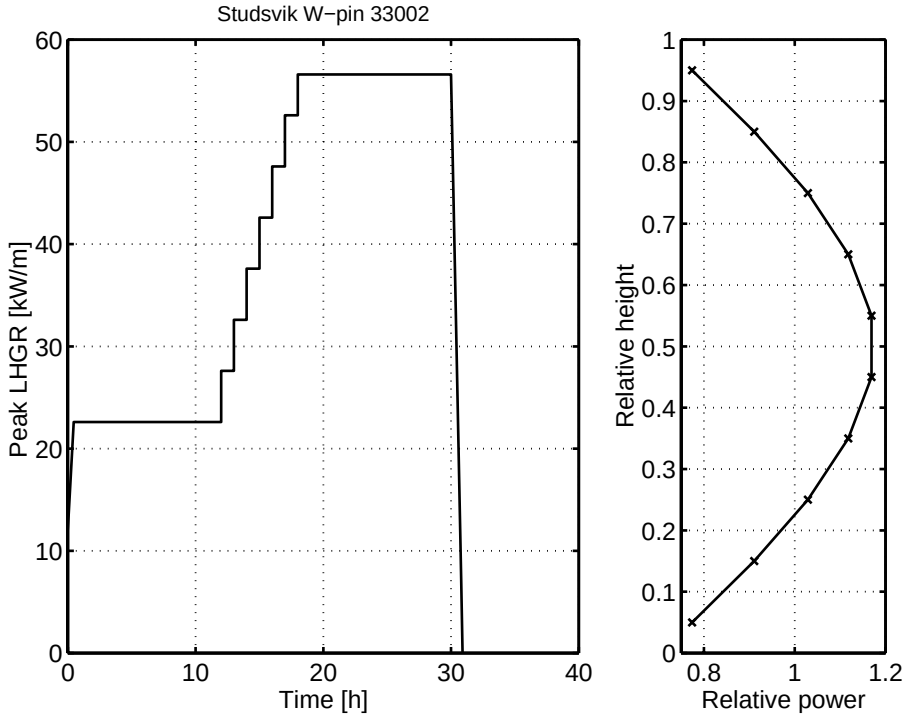

Figure 3. Ramp power history for the BWR pin and the axial power distribution along the fuel column.

After the ramp test, the pin underwent post-irradiation examination (PIE) in hot cell at Studsvik. The PIE included γ-spectrometry, pin diameter, pellet-clad gap size, fuel density and fission product gas release measurements. The γ-spectrometry was performed along the pin for determination of specific nuclides comprising ^{137}Cs and ^{134}Cs. The rod diameter measurements were made at 4 circumferential positions along the pin. The pellet-clad gap size of the pin was determined by compressing the rod transversally between two parallel flat edges and measuring the pin deformation as a function of applied force during the load cycle. The measurements were corrected for the elastic deformation of the apparatus. The relocated gap is measured when the applied force acting on the pellet reaches 50 N during the compression, whereas the compressed gap is chosen when the applied force against the pellet is decreased to 50 N during the decompression.

Fission product gas release was determined by first puncturing the pin in the plenum region, then measuring the internal gas pressure and determining the free volume. The amounts of released Xe and Kr gases were determined by mass spectroscopy analysis from retrieved samples. The fraction of fission gas release was determined by dividing the measured amount with the calculated amount of the generated inventory of these gases. Optical inspection of the clad inner surface revealed a large number of around 10 μm deep flaws, but no through-wall cracks. Table 2 lists pellet-clad gap size measurements, the relocated and compressed diametral gaps, including the data on clad outer diameter. Fig. 4 shows the profilometry data on clad diameter before and after ramp, and Fig. 5 displays the relocated gap size along the fuel. The released fraction of fission product gases Xe and Kr measured after ramp, the volumes and the corresponding pin internal pressure for this pin (W-pin 33002) are summarised in Table 3.

Table 1. Data on the 10×10 BWR assembly pin subjected to ramp test.

Fuel rod entity	As-fabricated	After base irradiation
Fuel pellet		
Material	UO_2	
Diameter, mm	8.25	8.34
Length, mm	10	not measured
Density, kgm^{-3}	10600	not measured
U-235 content, wt%	4.2	-
Cladding		
Material	Zircaloy-2/Sn-Zr liner	
	Full recrystallised annealed	
Outer diameter, mm	9.63	9.61
Wall thickness, mm	0.635	not measured
Pin		
Fill gas	helium	
Fill pressure at 293K, MPa	0.4	
Active length, mm	472	475.5
Plenum volume, mm^3	1560	not measured

3.2 PWR test

The PWR fuel power ramp experiment evaluated in our paper was performed on a segmented ABB Atom 17×17 PWR assembly rod, base irradiated in the Ringhals 3 PWR in Sweden, during years 1992-1994, to a rod exposure of about 27 MWd/kgU. The base power histories for the two considered segments (pins) are shown in Fig. 6. The two test pins of length 1054 mm with UO_2 fuel pellets were disassembled from the original (segmented)

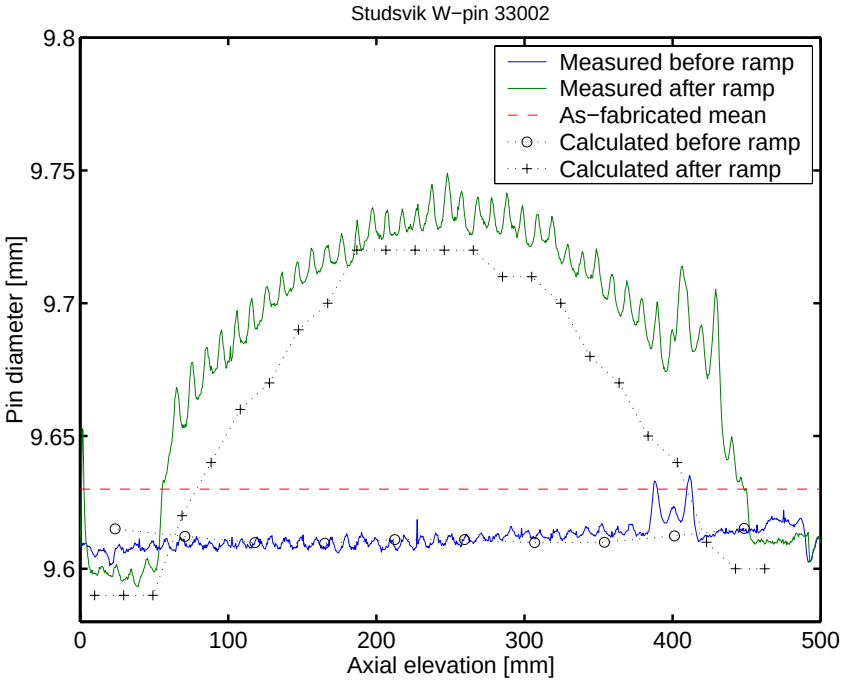

Figure 4. Comparison between measured and calculated clad outer diameter along the pin before and after ramp for the BWR pin.

Table 2. Data on the BWR pin after the ramp test.

Axial position from bottom	Relocated diametral gap	Compressed diametral gap	Cladding outer diameter
mm	μm	μm	mm
82	24	48	9.658
92	26	56	9.664
102	38	65	9.676
274.5	12	62	9.728
284.5	18	58	9.731
294.5	12	75	9.727
386	13	70	9.693
396	18	65	9.684
406	23	73	9.675

rod for power ramp testing in the Studsvik R2 reactor. The technical data on the fuel pin are presented in Table 4. The objective of this experiment was to compare the PCI resistance of PWR fuel with different clad materials irradiated to medium exposure.

More specifically, four pins of identical design, but two with Zircaloy-2 cladding and another two with Zircaloy-4 , all fabricated with identical thermal-mechanical treatment, were subjected to similar power ramp tests. The PWR loop number 1 of the Studsvik R2 reactor was used with typical PWR conditions (14.6 MPa, 588 K nominal inlet temperature). The first two tests, one pin with Zircaloy-2 cladding another with Zircaloy-4 cladding were ramped to a failure RTL, which showed to be around 48 kW/m. In the two remaining tests, the

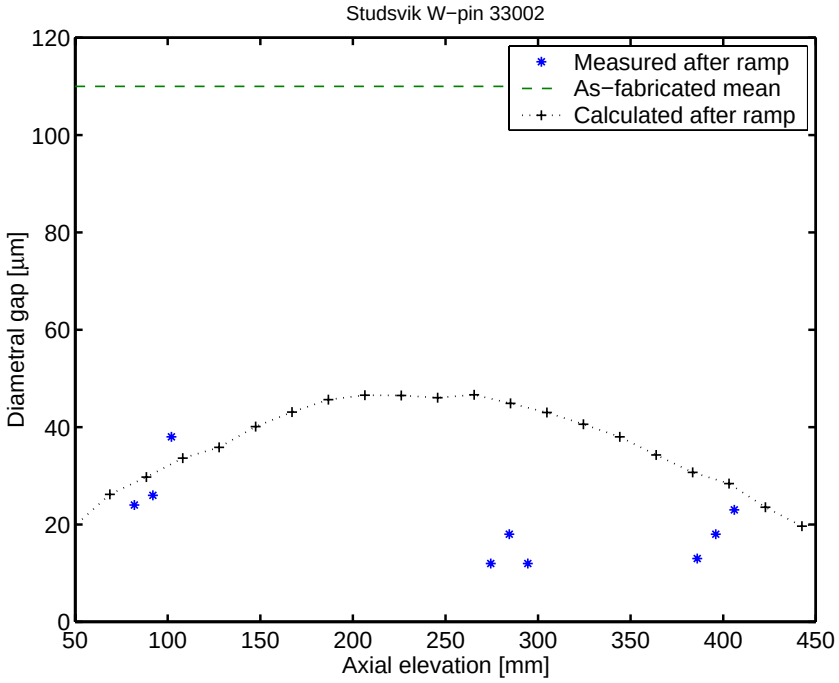

Figure 5. Comparison between measured and calculated pellet-clad gap along the fuel after the ramp for the BWR pin.

Table 3. Results of PIE on fission product gas release, volume and pressure of the BWR/PWR pins after the ramp tests. Volume values are at STP.

Quantity	W-pin 33002(BWR)	A-pin 30003(PWR)
Uranium mass, kg	0.233	0.493
Exposure, MWd/kgU	34	26.9
RTL, kWm^{-1}	56.5	41.3
Pin void volume, mm^3	4050	3900
He volume, mm^3	-	110700
Kr volume, mm^3	7246	1340
Xe volume, mm^3	62159	11500
Total gas volume, mm^3	84724	123500
Kr release fraction, %	28.9	3.1
Xe release fraction, %	30.4	3.3
Pin pressure (273.15 K), MPa	2.12	3.21

claddings remained intact after 12 h of hold time at RTL of 41 kW/m. According to Carlsson (1996) no difference in PCI performance of the two cladding materials, i.e. Zircaloy-2 vs. Zircaloy-4, could be seen. Here, we only analyse the Zircaloy-4 pins (A-pin 30002 & 30003).

The segment A-pin 30002 was ramped until failure occurred, whereas A-pin 30003 was ramped to below the failure power level in order to confirm the failure threshold. The power ramp was performed by rapidly increasing the linear power density of the pin from zero to 7 kW/m and then slowly up to 23 kW/m during 45 min. After 6 h hold time at the conditioning power level, the power was increased at a rate of 8-10 kW/m/min up to the RTL.

A-pin 30003 passed the 41 kW/m RTL with 12 h hold time, but A-pin 30002 failed at the higher 47.7 kW/m RTL after 5 min. The ramp power histories for the two pins are depicted in Fig. 7. This experiment, clearly, succeeded to demonstrate the threshold for PCI failure.

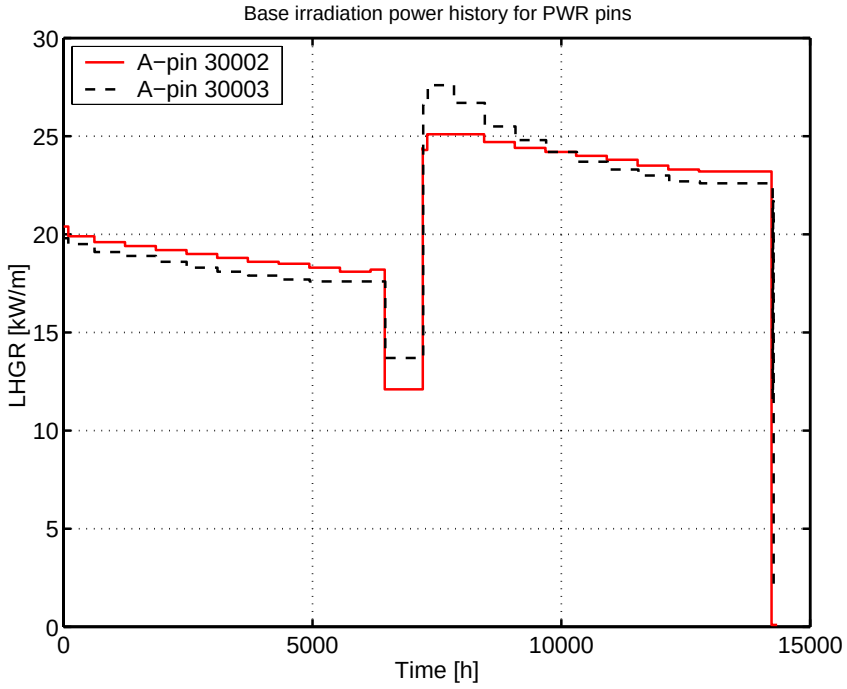

Figure 6. Base power histories for two PWR pins irradiated in the Ringhals 3 reactor.

As for the case of the BWR pin (W-pin 300002) discussed in the foregoing subsection, after the ramp tests, the pins underwent PIE in hot cell at Studsvik. The PIE included γ-spectrometry, pin diameter and pellet-clad gap size measurements, optical microscopy of clad inner surface and fission product gas release measurements that were made on the intact pin. Similar experimental procedures, as described for the BWR pin, were applied on these pins. The released fraction of fission product gases Xe and Kr (relative to gas produced in fuel) after ramp, the volumes and the corresponding rod internal pressure for the intact pin (A-pin 30003) are summarised in Table 3. Figure 8 shows several measured outer diameter data points obtained after the ramp for the intact rod A-pin 30003.

4 COMPUTATION AND ANALYSIS

The models described in the foregoing sections are included in the steady-state fuel rod thermal-mechanical code STAV. We used this code to evaluate the BWR and the PWR pins power ramped in the Studsvik R2 reactor. In the computations we have assumed that the pellet-clad effective friction coefficient is $\mu = 0.014$, see (Zhou et al. 2004). For fuel pellet swelling, due to production of solid fission products in fuel matrix, we have used the relation: $u_S = K_s R_p E$, where u_S is the pellet radial displacement due to swelling, K_s the swelling rate, R_p the initial (as-fabricated) pellet radius, and E the fuel exposure (Hagrman and Reyman 1979). No gaseous swelling model was employed. Furthermore, the following correlation for the pellet displacement due to relocation has been assumed (Forsberg and Massih 1989):

$$\frac{\mathrm{R}^m(E,q)}{R_p} = H(q-q_c)\mathrm{R}^\infty \mathscr{F}(E)\left(1-e^{-0.154(q-q_c)}\right), \tag{8}$$

$$\mathscr{F}(E) = 1-0.338\,e^{-0.15E}, \tag{9}$$

where q is the linear power density (kW/m), $q_c = 4$ kW/m, E the local exposure (MWd/kgU), $H(x)$ the Heaviside function, and R^∞ a calibration parameter deciding the asymptotic limit of pellet relocation (see below).

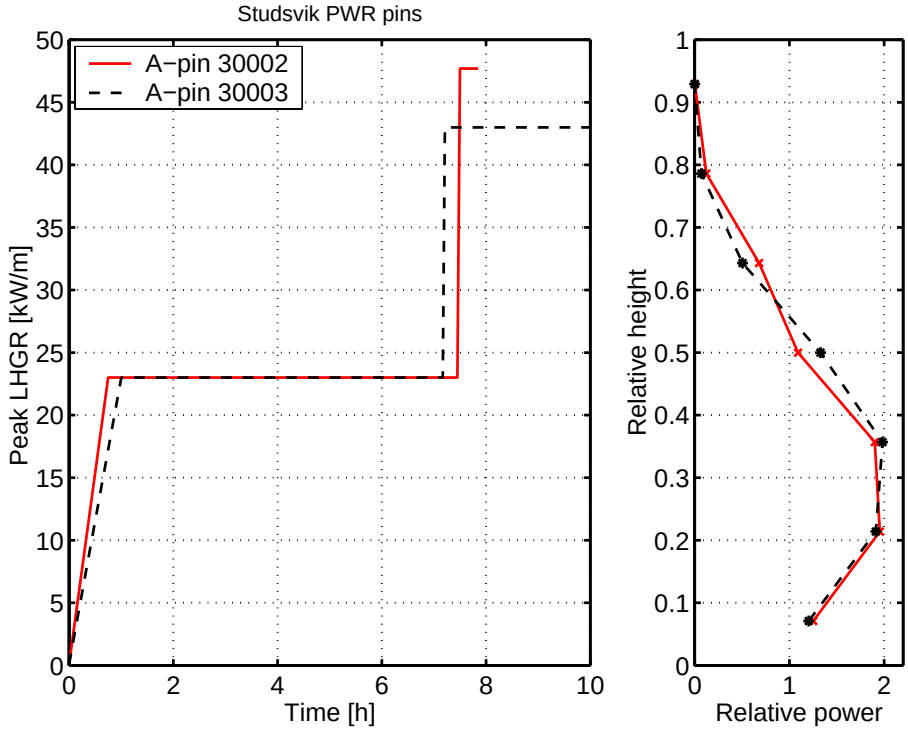

Figure 7. Ramp power history for the PWR pins and their axial power distributions along the fuel column. Note that A-pin 30002 failed after 5 min. at RTL, while A-pin 30003 survived the ramp and a 12 h hold time at RTL.

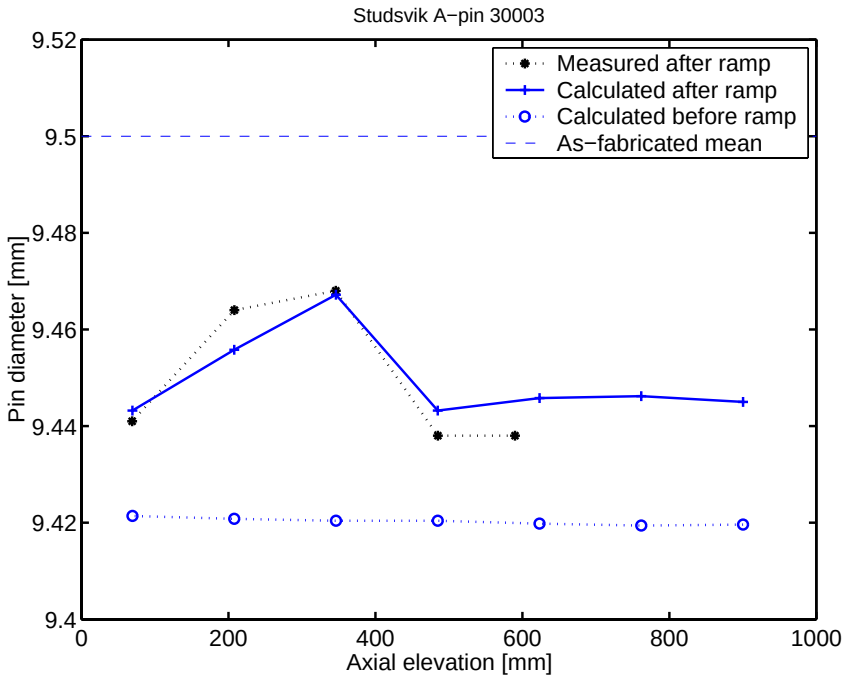

Figure 8. Comparison between measured and calculated clad outer diameter along the pin before and after ramp for the intact PWR pin. The measured data are only for after ramp.

Table 4. Data on the 17×17 PWR assembly pins subjected to ramp test.

Fuel rod entity	As-fabricated
Fuel pellet	
Material	UO_2
Diameter, mm	8.19
Length, mm	9
Density, kgm^{-3}	10500
U-235 content, wt%	3.6
Cladding	
Material	Zircaloy-4, stress relief annealed
Outer diameter, mm	9.5
Wall thickness, mm	0.5715
Pin	
Fill gas	helium
Fill pressure at 293K, MPa	2.5
Active length, mm	969.6
Plenum volume, mm^3	2000

4.1 BWR pin

For the ramp simulation of the BWR pin, nominal characteristic data (Table 1) were used as input. The pellet radial swelling rate was taken as $K_s = 2.0 \times 10^{-4}$ (MWd/kgU)$^{-1}$. The relocation parameters utilised are listed in Table 5, see Eqs. (1) and (8). The results are presented in terms of calculated clad outer diameter before and after ramp, together with measured data in Fig. 4. Figure 5 depicts the calculated relocated pellet-clad gap vs. measured values along the fuel pin. We observe from Fig. 4 that the clad outer diameter is somewhat underestimated after the ramp. This is mainly attributed to the gaseous fuel swelling during power ramp, which is not taken into account in the present simulation. We have neither modelled the thermal creep deformations of UO_2, which is expected to occur for $T > 0.5T_m$, with T_m being the melting temperature. The precise calculation of pellet-clad gap is very involved, since the pellets undergo complex cracking and distortion under the influence of temperature gradients during a ramp. Furthermore, the PCMI method utilised here is essentially a one-dimensional model, although the effect of axial forces on the clad is accounted for through a finite element method. Therefore, the occurrence of the pronounced clad ridging observed cannot be captured by 1-dimensional modelling of this effect, Fig. 4.

The peak hoop stress in the clad is calculated to be $\sigma_{\theta\theta}$= 710 MPa. The yield strength in that location of the clad is calculated to be 666 MPa. The calculated maximum hoop time-independent plastic strain is about 0.1%, which is much lower than the calculated failure strain of about 1.45%, see Eq. (7). Consequently, the rod survival is accurately calculated for this case. Moreover, our calculations show that the maximum stress intensity at the observed 10 μm deep flaws at the clad inner surface is 4.9 MPam$^{1/2}$. The base irradiation fission gas release fraction is calculated to be around 0.3%, while the value after the ramp is calculated as 34.5%, which is close to the measured value of 32%. It is worth noting that the calculated values presented in this subsection slightly differ with the values we reported earlier (Zhou et al. 2004). This because of the new re-calibration of the STAV code with the extended Westinghouse database.

4.2 PWR pins

For the ramp simulation of the two PWR pins, nominal characteristic data (Table 4), except for fuel pellet diameter, were used as input. For the pellet outer diameter, it was judged that the uncertainty in pellet radius needs to be taken into account; thus we used $R_p = 4.10$ mm. Also a higher value for the pellet swelling rate than for the case of BWR pin was assumed, namely, $K_s = 2.75 \times 10^{-4}$ (MWd/kgU)$^{-1}$. We note that this value is still lower than

Table 5. Relocation parameters utilised in present computations, see Eqs. (1) and (8).

Parameter	BWR rod	BWR pin	PWR rod	PWR pins
	Steady-state	Ramp	Steady-state	Ramp
P_n^m, MPa	40	200	40	800
R^∞	6.0×10^{-3}	7.55×10^{-3}	6.0×10^{-3}	7.55×10^{-3}

the values reported in literature (Assman and Manzel 1977), which is $K_s = (3.33 \pm 0.5) \times 10^{-4}$ (MWd/kgU)$^{-1}$. The relocation parameters utilised are listed in Table 5. Note that the relocation parameters are selected to be greater for the ramp case than for the base irradiation (steady-state), in particular for PWR pins regarding P_n^m, see Eq. (1). By this doing, we obtain a better agreement between calculated and measured clad deformation.

The results of our computations are presented in terms of calculated clad outer diameter before and after ramp together with measured data after ramp for the survived pin (A-pin 30003) in Fig. 8. It is seen that by using the aforementioned choice of input parameters the calculated clad deformations after ramp are in agreement with measured values. The maximum calculated permanent (creep + plastic) clad hoop strain during ramp is about 0.5%. By comparing Figs. 4 and 8, we observe that the PWR clad experienced much more creep-down than the BWR clad during the base irradiation, as it is anticipated.

For A-pin 30003, the peak clad hoop stress under ramp is calculated to be $\sigma_{\theta\theta}$= 721 MPa. The yield strength in that location of the clad is calculated to be 656 MPa. The calculated maximum hoop (time-independent) plastic strain is 0.11%. Our calculations also show that the maximum stress intensity at the observed 10 μm deep flaws at the clad inner surface is 4.9 MPam$^{1/2}$. The base irradiation fission gas release fraction is calculated to be around 0.1%, while the value after the ramp is calculated as 5.3%, which is somewhat above the measured value of 3.3%. The calculated Xe and Kr volumes (at STP) released after ramp are 17965 mm^3 and 1996 mm^3, respectively, which are again larger than the measured values, see Table 3.

For the failed pin (A-pin 30002), the clad hoop plastic strain is calculated to be 0.29%, which is much larger than the corresponding value calculated for A-pin 30003. At this level of plastic deformation the clad peak hoop stress is calculated to be $\sigma_{\theta\theta}$= 666 MPa, which is lower than the value calculated for the intact pin. This is attributed to stress relaxation under a larger plastic deformation of A-pin 30002 clad. The yield strength in that location of the clad is calculated to be 647 MPa. The calculated value for the maximum clad stress intensity is 4.6 MPam$^{1/2}$ close but smaller than the value computed for A-pin 30003.

Our analysis shows that both PWR pins suffer from stress corrosion cracking. However, in neither of the pins the crack propagated through the clad wall, i.e. they both got arrested. Computations with higher resolutions of stresses and strains as a function of time during power ramps are needed to settle this discord with the experimental results.

5 CONCLUSIONS

With the aid of models presented in this paper, we have been able to simulate fairly well the observed pellet-clad interaction behaviour under certain power ramp tests made on BWR and PWR fuel pins. In our simulation of the BWR pin, we retrodicted measured values of clad deformation and fission product gas release satisfactorily. Also our calculations of these attributes for the PWR pin are retrodicted fairly, despite significant differences in the ramp power history and ramp terminal level of the considered tests. The ramp terminal level for the BWR pin was 56.5 kW/m with measured fission gas release fraction of 32%. Our computation retrodicted 34.5% release. For the survived PWR pin, RTL was 41 kW/m and measured fission gas release 3.2%. Our computation yielded 5.3% release. In order to capture the measured values of clad deformation, we enhanced the best-estimate values of fuel swelling rate as well as the relocation model parameter. The reason for this deed could be due to the fact that we have not modelled gaseous swelling during power ramp. For the BWR pin with liner, our clad failure model provided an acceptable retrodiction of clad survivability. The hoop plastic strain was calculated as 0.1%, while the failure strain was calculated as 1.45%. Our failure analysis indicated that both PWR pins suffered from stress corrosion cracking. However, in neither of the pins the crack propagated through the clad wall. Computations with higher resolutions of stresses and strains as a function of time during power ramps are needed to resolve this disagreement with the experimental results. We hope to include the effect of gaseous swelling and a more refined stress-strain computation in a future study.

REFERENCES

Armijo, J. S., Coffin, L. F. and Rosenbaum, H. S.: 1994, Development of zirconium barrier fuel cladding, *Zirconium in the Nuclear Industry (Tenth International Symposium)*, Vol. ASTM STP 1245, Philadelphia, PA, USA, pp. 3–18.

Assman, H. and Manzel, J.: 1977, The matrix swelling rate of UO_2, *Journal of Nuclear Materials* **68**, 360–364.

Billaux, M.: 2004, Modelling pellet-cladding mechanical interaction and application to BWR maneuvering, *Proceedings of the 2004 International Meeting on LWR Fuel Performance*, American Nuclear Society, Orlando, Florida. 19-22 September, 2004.

Carlsson, M.: 1996, Power ramp testing on four ABB atom PWR segments, *Technical Report N(R)-96/050*, Studsvik Nuclear, Nyköping, Sweden.

Carlsson, M. and Engman, U.: 1999, Test facility and experimental technique for fuel rod ramps, *Technical Report N(R)-99/063*, Studsvik Nuclear, Nyköping, Sweden.

Cox, B.: 1990, Pellet-cladding interaction failures of zirconium alloy fuel cladding, *Journal of Nuclear Materials* **172**, 242–292.

Dahlbäck, M., Halstadius, L. and Limbäck, M.: 2004, The effect of liner component iron content on cladding corrosion, hydriding and PCI resistance, *Zirconium in the Nuclear Industry (Fourteenth International Symposium)*. To be published.

Edsinger, K. and Murthy, K. L.: 2001, LWR pellet-cladding interactions: material solutions to SCC, *JOM* **53**, 9–13.

Forsberg, K. and Massih, A. R.: 1989, A model for pellet-clad gap conductance, *Water reactor Fuel Element Computer Modelling in Steady-State, Transient and Accident Conditions*, IAEA, Vienna, Austria. Publication IWGFPT/32.

Forsberg, K. and Massih, A. R.: 2001, Theory of fission gas release during grain growth, *Transactions of SMiRT 16*, Washington DC. August 2001.

Fuhrman, N., Pasupathi, V. and Corsetti, L.: 1977, PCI observation in a Combustion Engineering PWR, *ANS Topical Meeting on Water Reactor Fuel Performance*, American Nuclear Society. St. Charles, Illinois, May 1977.

Fuhrman, N., Pasupathi, V. and Scott, D. B.: 1976, Evaluation of of fuel rod performance in Main Yankee core-1, *Technical report*, EPRI, Palo Alto, California.

Gärtner, M. and Fischer, G.: 1987, Survey of the power ramp performance testing of KWU's PWR UO_2 fuel, *Journal of Nuclear Materials* **149**, 29–40.

Hagrman, D. L. and Reyman, G. A.: 1979, MATPRO 11 Handbook, *Technical Report NUREG/CR-0497*, USNRC.

Jernkvist, L. O.: 1995, A model for predicting pellet-cladding interaction-induced fuel rod failure, *Nuclear Engineering and Design* pp. 393–399.

Jernkvist, L. O.: 2005, PCI failure criteria for liner and non-liner fuel rods, *Technical Report TR05-002*, Quantum Technologies, Uppsala, Sweden.

Jernkvist, L. O., Massih, A. R. and Rudling, P.: 2004, A strain-based clad failure criterion for reactivity initiated accidents in light water reactors, *Technical Report 2004:32*, Swedish Nuclear Power Inspectorate, Stockholm, Sweden.

Limbäck, M. and Andersson, T.: 1996, *Zirconium in the Nuclear Industry*, Vol. ASTM STP 754, American Society for Testing and Materials, W. Conshohocken, Pennsylvania.

Massih, A. R., Hallstadius, L. and Vesterlund, G.: 1987, PCI-resistance of Zr-Sn liner fuel, *Technical Report UK 87-559*, ABB Atom, Västerås, Sweden.

Massih, A. R., Rajala, T. and Jernkvist, L. O.: 1995, Analyses of pellet-cladding mechanical interaction behaviour of different ABB Atom fuel rod designs, *Nuclear Engineering and Design* **156**, 383–391.

Ohara, H., Nomata, T., Irube, M., Iwata, S. and Futakuchi, M.: 1994, Fuel behavior during power ramps, *1994 International Topical Meeting on LWR Fuel Performance*, West Palm Beach, Florida.

Speight, M. V.: 1969, A calculation on the migration of fission gas in material exhibiting precipitation and resolution of gas atoms under irradiation, *Nuclear Science and Engineering* **37**, 180–185.

Zhou, G., Lindbäck, J. E., Schutte, H. C., Jernkvist, L. O. and Massih, A. R.: 2004, Modelling of pellet-clad interaction during power ramps, *International Seminar on Pellet-Clad Interaction in Water Reactor Fuels*, Aix en Provance, France. 9-11 March, 2004.